Probing the Role of E272 in Quinol Oxidation of Mitochondrial Complex III†

Tina Wenz,‡ Petra Hellwig,§ Fraser MacMillan,|| Brigitte Meunier,⊥ and Carola Hunte*,‡

Department Molecular Membrane Biology, Max-Planck-Institute of Biophysics, 60438 Frankfurt am Main, Germany, Institute for Biophysics, Johann-Wolfgang-Goethe-University, 60438 Frankfurt am Main, Germany, Institute for Physical and Theoretical Chemistry and Center for Biomolecular Magnetic Resonance, Johann-Wolfgang-Goethe-University, D-60439 Frankfurt am Main, Germany, and Wolfson Institute for Biomedical Research, University College London, London WCIE6BT, U.K.

Received February 9, 2006; Revised Manuscript Received May 2, 2006

ABSTRACT: Bifurcated electron transfer during ubiquinol oxidation is the key reaction of complex III catalysis, but the molecular basis of this process is still not clear. E272 of the conserved cytochrome *b* PEWY motif has been suggested as a ligand and proton acceptor for ubiquinol oxidation at center P. We introduced the two replacement mutations, E272D and E272Q, into the mitochondrially encoded cytochrome *b* gene by biolistic transformation to study their effects on substrate binding and catalysis. Both substitutions resulted in a lower ubiquinol cytochrome *c* reductase activity and affect the K_M for ubiquinol. The E272 carboxylate stabilizes stigmatellin binding, and in accordance, both variants are resistant to stigmatellin. Large structural changes in the cofactor environment as well as in the binding pocket can be excluded. The mutations do not perturb the midpoint potentials of the heme groups. The sensitivity toward the respective distal and proximal niche inhibitors HDBT and myxothiazol is retained. However, both mutations provoke subtle structural alterations detected by redox FTIR. They affect binding and oxidation of ubiquinol, and they promote electron short-circuit reactions resulting in production of reactive oxygen species. The aspartate substitution modifies the environment of the reduced Rieske protein as monitored by EPR. Both variants alter the pH dependence of the enzyme activity. Diminished activity at low pH coincides with the loss of one protonatable group with a pK_a of ∼6.2 compared to three pK_a values in the wild type, supporting the role of E272 in proton transfer. The conserved glutamate appears to influence the accurate formation of the enzyme−substrate complex and to govern the efficiency of catalysis.

Mitochondrial complex III is a central component of respiratory energy conversion. The homodimeric complex, also termed ubiquinol:cytochrome *c* oxidoreductase (QCR),[1] resides in the inner mitochondrial membrane. Each monomer comprises three catalytic subunits: the Rieske iron−sulfur protein (ISP), cytochrome c_1, and cytochrome *b*. The latter is encoded by the mitochondrial genome. In the yeast enzyme, seven additional subunits per monomer are attached to this catalytic core (*1*, *2*). QCR catalyzes the transfer of electrons from the membrane-localized ubiquinol to the water-soluble cytochrome *c*. This redox reaction is coupled to the translocation of protons across the membrane. The mechanism described by the protonmotive Q-cycle depends on two spatial separated quinol/quinone binding sites (*3*) (Figure 1a). The key step of the mechanism is the bifurcated route of the two electrons released upon ubiquinol oxidation at center P. One electron is transferred into the high-potential chain consisting of ISP, cytochrome c_1, and cytochrome *c*. The second electron is transferred via the low-potential chain, namely, heme b_L and heme b_H of cytochrome *b*, to center N at which quinone is reduced to semiquinone. A complete turnover of the enzyme requires the oxidation of two ubiquinol molecules, resulting in full reduction of the semiquinone. The electron transfer to cytochrome c_1 involves a large movement of the ISP head domain (*4*, *5*). Reduction of ISP occurs in its *b*-position docked onto cytochrome *b*, and a movement toward cytochrome c_1 facilitates electron transfer to the latter.

The molecular mechanism of ubiquinol oxidation is under debate. Several hypotheses for explaining the divergent transfer of electrons into thermodynamically different pathways have been proposed (*5*−*7*). The position and dimension of the ubiquinol binding pocket have been deduced from QCR structures with well-characterized center P-specific inhibitors, which bind to overlapping niches in the bilobal pocket distal and proximal to heme b_L (*1*, *8*−*11*). The enzyme−substrate complex consists of cytochrome *b*, ubiquinol, and ISP; however, its molecular structure is not known (*5*−*7*). E272 of the highly conserved cytochrome *b* PEWY motif (*12*) and H181 of ISP are discussed as direct

† This work was supported by the DFG (SFB 472) and Boehringer Ingelheim Fonds.

* To whom correspondence should be addressed: Max-Planck-Institute of Biophysics, Max-von-Laue-Str. 3, 60438 Frankfurt am Main, Germany. Telephone: +49 (0) 69 6303 1062. Fax: +49 (0) 69 6303 1002. E-mail: Carola.Hunte@mpibp-frankfurt.mpg.de.

‡ Max-Planck-Institute of Biophysics.

§ Institute of Biophysics, Johann-Wolfgang-Goethe-University.

|| Institute for Physical and Theoretical Chemistry and Center for Biomolecular Magnetic Resonance, Johann-Wolfgang-Goethe-University.

⊥ University College London.

[1] Abbreviations: QCR, ubiquinol:cytochrome *c* oxidoreductase; ISP, Rieske iron−sulfur cluster; UHDBT, 5-*n*-undecyl-6-hydroxy-4,7-dioxobenzothiazole; THDBT, 5-*n*-tridecyl-6-hydroxy-4,7-dioxobenzothiazole; UM, *n*-undecyl β-d-maltoside; PMSF, phenylmethylsulfonyl fluoride; RCR, respiratory control rate; DQH, decylubiquinol.

10.1021/bi060280g CCC: $33.50
Published on Web 07/07/2006

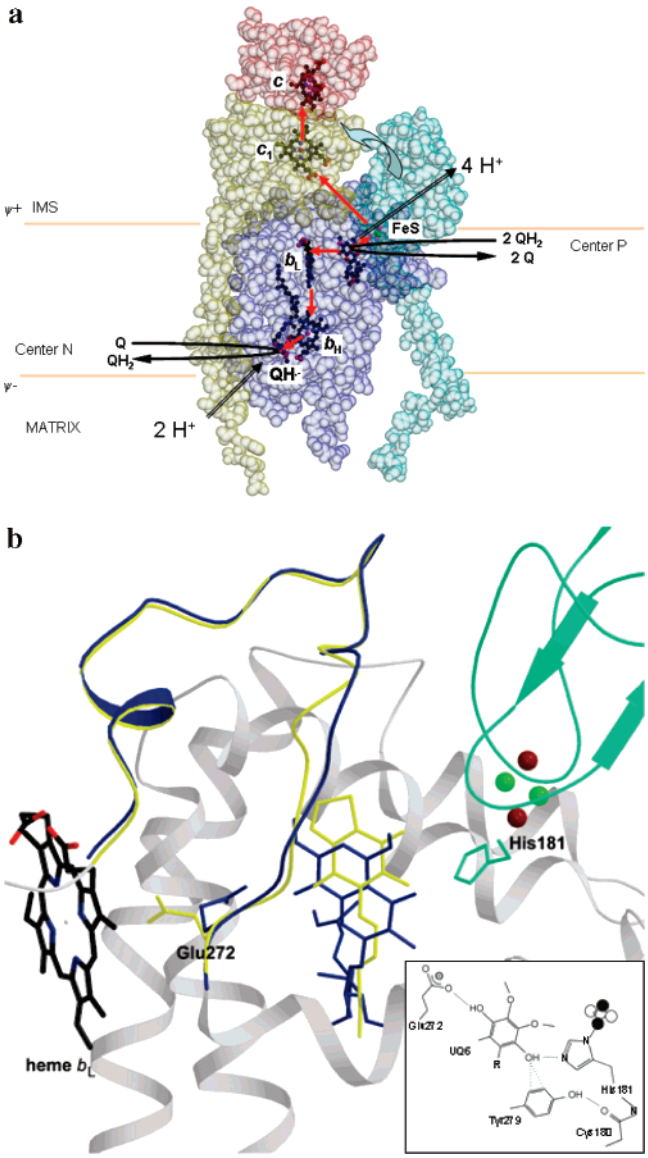

FIGURE 1: (a) Catalytic core of QCR and scheme of the Q-cycle. The subunits cytochrome *b* (blue), ISP (green), and cytochrome c_1 (yellow) are shown in transparent surface presentation with their respective cofactors. The [2Fe-2S] cluster of ISP is presented as green and magenta balls, and the phospholipid bilayer is denoted with orange lines. Red arrows depict electron transfer, and black double-lined arrows mark proton uptake and release at center N and center P, respectively. The inhibitor stigmatellin is bound at center P. The coordinates [PDB entry 1KYO (*45*)] of yeast QCR with bound cytochrome *c* have been used. (b) Inhibitor and substrate binding at center P. Structures of yeast QCR with bound stigmatellin [blue, PDB entry 1EZV (*1*)] and HHDBT [yellow, PDB entry 1P84 (*9*)] have been superimposed. Both inhibitors are stabilized by hydrogen bonds with E272 of cytochrome *b* and H181 of ISP. The proposed enzyme−substrate complex with ubiquinol is shown in the inset with E272 and H181 as ligands and Y279 for positioning of the substrate in the binding site (according to ref *9*).

ligands of ubiquinol and as primary acceptors for the protons released upon ubiquinol oxidation [numbering of residues according to yeast; Figure 1b (*1*, *9*, *13*, *14*)]. The rotational displacement of E272 observed in QCR structures with different inhibitors or with nonoccupied center P (*1*, *4*, *9*, *15*) led to the proposal that E272 upon protonation rotates toward heme b_L, facilitating a thermodynamically favorable coupled proton−electron transfer in that direction, the initial step for proton release (*1*, *9*, *13*, *14*). A recent conformational gating model integrates E272 as a switch, which directs the stabilization of substrate and reaction intermediates by appropriate side chain conformation (*16*).

We substituted glutamate at position 272 of mitochondrial cytochrome *b* from the yeast *Saccharomyces cerevisiae* with aspartate and glutamine to question the importance of the exact side chain position and of its protonation capacity for substrate binding and ubiquinol oxidation. The detailed characterization of the variants supports the importance of E272 for center P catalysis.

EXPERIMENTAL PROCEDURES

Media and Yeast Strains. Premixed media were from ForMedium. YPD [1% (w/v) yeast extract, 2% (w/v) peptone, and 3% (w/v) glucose] and YPG [1% (w/v) yeast extract, 2% (w/v) peptone, and 3% (w/v) glycerol] were used for growth of the yeast strains. The transformation medium [0.7% (w/v) yeast nitrogen base, 3% (w/v) glucose, and 2% (w/v) agar, 1 M sorbitol, and 0.8 g/L complete supplement mixture without uracil supplied from Anachem] was used for the biolistic transformation. The recipient strain for biolistic transformation was W303-1B/rho^0 (Mat α; ura 3−52, trp 1Δ2, leu 2−3_112, his3−11, ade2−1, can 1−100 [no mt DNA]). The mit$^-$ tester strains were CKL65 (Mat a, leu1, kar1−1 [mit$^-$ Cytb T46K]) and CKL57 (Mat a, leu1, kar1−1 [mit$^-$ Cytb L263stop]) with a rho$^+$ intronless mitochondrial DNA. Wild-type strain CKWT was Mat a, leu1, kar1−1.

Site-Directed Mutagenesis, Biolistic Transformation, and Selection of Mitochondrial Mutants. Plasmid pBM5 carrying the wild-type intronless sequence of the cytochrome *b* gene was mutagenized using the Quick Change site-directed mutagenesis kit (Stratagene). The following primers were used: 5′-CAT CTA TGG TAC CTG AAT GAT ACT TAT TAC-3′ and 5′-GTA ATA AGT ATC ATT CAG GTA CAA TAG ATG-3′ for E272D and 5′-CAT CTA TGG TAC CTC AAT GAT ACT TAT TAC-3′ and 5′-GTA ATA AGT ATC ATT GAG GTA CAA TAG ATG-3′ for E272Q. The exchange was verified by sequencing. The mitochondrial biolistic transformation by microprojectile bombardment was adapted from ref *17*. Three micrograms of the plasmid carrying the mutated cytochrome *b* gene and 0.5 μg of YEP352 plasmid (which contains the URA3 gene, allowing the selection of Ura$^+$ nuclear transformants) were mixed with 50 μL of 0.7 μm tungsten particles at a concentration of 60 mg/mL. The particles (Bio-Rad) were prepared and coated with DNA according to the manufacturer's protocol. Aliquots of the coated particles were used for the transformation of recipient strain W303-1B/rho^0. Approximately 10^7 cells of the recipient strain were evenly spread on transformation medium that is selective for Ura$^+$ transformants. The particle bombardment was performed with a Biolistic PDS 1000/He particle delivery system (Bio-Rad), according to the manufacturer's recommendation.

Colonies of Ura$^+$ transformants, which have received the YEP352 plasmid, appeared after 4−5 days. Mitochondrial transformants (or synthetic rho$^-$ clones) were identified by crossing the Ura$^+$ colonies with respiratory-deficient (mit$^-$) tester strain CKL65 (CobpT46K). Since the tester deficiency mutation could be corrected by recombination with the plasmid-derived mitochondrial sequence, mitochondrial trans-

formants were identified by their ability to form respiratory-competent diploids when crossed with the tester strain. The mitochondrial transformants were then subcloned and tested again.

For integration of the E272D mutation into the mitochondrial genome, the mitochondrial transformant (synthetic rho$^-$) was crossed to mit$^-$ tester strain CKL57 (Cobp L263stop). Respiratory-competent diploids were subcloned, and integration of the mutation into the cytochrome *b* gene was verified by sequencing.

The E272Q mutation was integrated into the mitochondrial DNA by crossing of the mitochondrial transformant to wild-type strain CKWT (*18*, *19*). Diploids that exhibited a slow growth phenotype on YPG were subcloned, and integration of the mutation into the cytochrome *b* gene was verified by sequencing.

Purification of QCR. Wild-type and mutant yeast strains were grown in YPG medium and harvested at late logarithmic phase. Mitochondrial membranes were prepared of a 60% (w/v) cell suspension in 250 mM sucrose, 50 mM potassium phosphate buffer (KP_i) (pH 7.3), 1 mM PMSF, 5 mM EDTA, and 2% (w/v) BSA in a cell mill equipped with glass beads (0.5 mm diameter). Cell debris was separated at 5000*g* for 45 min. Membranes were collected from the supernatant by ultracentrifugation at 150000*g* for 60 min. The membranes were stored at −80 °C until further use.

QCR was purified via two consecutive DEAE anion exchange chromatographic steps as described previously (*20*). Membranes were solubilized at a protein concentration of 10 mg/mL with 1.5% dodecyl maltopyranoside. The detergent was exchanged with 0.05% (w/v) undecyl maltopyranoside (UM) at the second DEAE step. Extinction coefficients of 17.5 mM^{-1} cm^{-1} for *c* heme (553−540 nm, ascorbate/ferricyanide) and 25.6 mM^{-1} cm^{-1} for *b* hemes (562−575 nm, dithionite/ferricyanide) were used for redox-spectroscopic quantification of QCR.

Reconstitution of Purified QCR. Purified QCR was reconstituted in soy asolectin in a 1/10 protein/lipid molar ratio. Detergent was removed by dialysis for 24 h against 100 mM KCl and 3 mM Hepes-KOH (pH 7.2).

Ubiquinol-Cytochrome c Reductase Activity Assay. The ubiquinol-cytochrome *c* reductase activity of purified QCR was assayed in 50 mM KP_i (pH 7.4), 250 mM sucrose, 1 mM KCN, 0.05% UM, and 50 μM horse heart cytochrome *c* at room temperature. The enzyme was diluted to 2.5−10 nM in the assay buffer, and the reaction was started with 40 μM decylubiquinol (DQH). Reduction of cytochrome *c* was monitored at 550−540 nm in dual-wavelength mode, and the rate of cytochrome *c* reduction was calculated with an extinction coefficient of 21.5 mM^{-1} cm^{-1}. For estimation of superoxide anion generation, the assay was supplemented with 50 units/mL catalase in the absence and presence of 50 units/mL CuZnSOD. The rate of superoxide anion formation is equal to the SOD-sensitive rate of cytochrome *c* reduction.

Activity assays of reconstituted QCRs were carried out in 100 mM KCl, 3 mM Hepes-KOH (pH 7.2), 1 mM KCN, 2 μg/mL valinomycin, 40 μM decylubiquinol, and 50 μM horse heart cytochrome *c* using 2.5−10 nM QCR. Turnover numbers have units of moles of cytochrome *c* reduced per mole of QCR per second under steady-state conditions.

Determination of K_m Values of DQH. Variable concentrations of DQH were used as substrate in the activity assay with the reconstituted enzyme. The concentration of the DQH stock solution was spectroscopically estimated at the start of the experiment. K_m values were obtained by linear regression in an Eadie−Hofstee plot.

Inhibitor Titrations. Reconstituted QCR was mixed with variable concentrations of inhibitor to yield different inhibitor/QCR ratios. The mixture was incubated for 15 min at room temperature before the activity assay was started as described above. QCR was pre-reduced with DQH for titration with 5-*n*-heptyl-6-hydroxy-4,7-dioxobenzothiazole (HHDBT), and the reaction was started with cytochrome *c*. The concentration of the inhibitors was determined by their extinction coefficient (*8*). Dilutions were carried out freshly just before the titrations.

Determination of the H^+/e^- Stoichiometry. The H^+/e^- stoichiometry was determined by the oxidant-pulse method (*20*, *21*) with the following modifications. Purified QCR was reconstituted as described above and dialyzed against 103 mM KCl and 10 μM Hepes-KOH (pH 7.2). The respiratory control rate (RCR) of the reconstituted QCR was determined as the ratio of the turnover number in the presence and absence of 10 μM carbonyl cyanide *m*-chlorophenylhydrazone (CCCP). Reconstituted QCR was quantified by redox spectroscopy and diluted to 0.8 μM cytochrome c_1. Decylubiquinol (40 μM), valinomycin (2 μg/mL), horse heart cytochrome *c* (12 μM), and phenol red (3.4 μM) are added to the reconstituted QCR, and the pH is adjusted to 7.2 by addition of HCl or NaOH. Ferricyanide (5−10 μM) is added, and the acidification is followed at 558−593 nm. Each pulse experiment is calibrated by addition of 5−10 μM NaOH.

Determination of the Turnover Number at Different pH Values. The assay was carried out according to ref *23* with a few modifications. Purified QCR was diluted to a concentration of 1 μM in a buffer containing 50 mM KP_i, 250 mM NaCl, and 0.05% UM. The ubiquinol:cytochrome *c* reductase activity of 10 nM QCR and 30 μM horse heart cytochrome *c* was measured in assay medium containing 0.05% UM and one of the following buffers at 20 mM: citric acid, Mes, Hepes, and Taps. The pH of the solution was adjusted with KOH from 5 to 9.5 with intervals of 0.25 unit. The reaction was started by addition of 4, 8, 16, 24, and 32 μM DQH, and the turnover number was corrected by the nonenzymatic activity. The data were plotted and fitted using ORIGIN 5.0 (OriginLab Corp.).

EPR Spectroscopy. Purified QCR (20 μM) in 50 mM KP_i (pH 6.9), 250 mM NaCl, and 0.05% UM was reduced by addition of excess pyrophosphate-buffered sodium dithionite at 4 °C, and the samples were immediately transferred to EPR tubes (standard suprasil quartz, outside diameter of 4 mm) and frozen in liquid nitrogen.

X-Band (9.4 GHz) continuous-wave (cw) EPR spectra were measured on a Bruker E500 ELEXSYS spectrometer using a standard rectangular Bruker resonator. The microwave frequency and magnetic field were measured using an external frequency counter and a Bruker field controller, respectively. The instrument was equipped with an Oxford helium cryostat (ESR900). The X-band spectra were simulated using Win-Simfonia. The measured *g* values were corrected for an offset against a known *g* standard (DPPH, for which $g = 2.00351 \pm 0.00002$).

Table 1: Properties of Wild-Type, E272Q, and E272D Yeast Strains and of the Respective Purified QCRs[a]

	wild type	E272Q	E272D
doubling time on respiratory medium (h)	3.2 ± 0.2	9.4 ± 0.3	3.4 ± 0.1
QCR content [mg/mL mitochondrial membranes] (wt %)	3.43 ± 0.32 (100)	1.98 ± 0.21 (58)	1.65 ± 0.18 (48)
TN (s^{-1}) (wt %)	52.1 ± 5.0 (100)	6.9 ± 1.0 (13)	25.8 ± 2.6 (49)
K_m(DQH) (μM)	6.3 ($R^2 = 0.91$)[b]	3.2 ($R^{2a} = 0.89$)	0.9 ($R^2 = 0.92$)[b]
I_{50}^r(stigmatellin)	1	resistant	resistant
I_{50}^r(HHDBT)	1	0.57	0.75
H^+/e^-	2.01 ± 0.07	1.97 ± 0.12	1.98 ± 0.15

[a] The doubling time was measured in complete medium with 3% glycerol (YPG) for three individual cultures per strain. The QCR content was determined in mitochondrial membranes by redox-spectroscopic quantification of the *b*-type hemes for three membrane preparations (see Experimental Procedures). The turnover number (TN) was detected as the cytochrome *c* reductase activity of the purified enzymes as described in Experimental Procedures. Three preparations per strain were used, and the activity measurements were repeated five times for each sample. The average error is within 10% of the given value. The K_m value was determined with an Eadie−Hofstee plot of the activity against the quotient of activity and DQH concentration. The parameter K_m for decylubiquinol (DQH) and the relative inhibitor values [$I_{50}^r = IC_{50}$(mutant)/IC_{50}(wild type)] were determined for QCR reconstituted in liposomes. Measurement of the H^+/e^- stoichiometry was carried out by the oxidant-pulse method using reconstituted QCR. The RCRs of the vesicles were between 3.3 and 4.5. Each pulse experiment was carried out six to eight times with two different enzyme preparations. [b] R^2 is the correlation coefficient of the linear regression.

Spectroelectrochemistry. An ultrathin layer spectroelectrochemical cell for the VIS and IR was used as previously described (*24*). Detergent-solubilized purified QCR was used at a concentration of ~70 mg/mL. Sufficient transmission in the 1800−1000 cm^{-1} range, even in the region of strong water absorbance around 1645 cm^{-1}, was achieved with the cell path length set to 6−8 μm. The gold grid working electrode was chemically modified with a 2 mM cysteamine and mercaptopropionic acid solution in a ratio of 1/1, and 16 different mediators were added as reported previously (*25*) to a final concentration of 45 μM each {except *n*-methyl- and *n*-ethylphenazonium sulfate, but adding neutral red [E_m = −307 vs the SHE (*26*)]} to accelerate the redox reaction. At this concentration, and with a cell path length of <10 μm, no spectral contributions from the mediators in the visible and infrared range could be detected in control experiments with samples lacking the protein, except for the PO modes of the phosphate buffer between 1200 and 1000 cm^{-1}. Potentials were measured with a Ag/AgCl/3 M KCl reference electrode and are quoted in reference to the SHE (pH 7).

The redox titrations were performed by stepwise setting the potential steps and recording the spectrum after equilibration. Typically, data were recorded at steps of 40 mV between −0.4 and 0.2 V. All measurements were performed at 5 °C. The pH was adjusted in Tris buffer (pH 7.5). The reference electrode was calibrated with the cyclovoltammogram of a buffered $K_4[Fe(CN)_6]$ solution before the potential titration was started. All electrochemical titrations were reversible as controlled by directly comparing fully oxidized minus fully reduced visible spectra at different points in the experiments. Data analysis was carried out with a program developed by S. Grzybek termed EHTIT (*27*); the midpoint potentials (E_m) and the number (*n*) of transferred electrons are obtained by adjusting a calculated Nernst curve to the measured absorbance change at a single wavelength, using the best fit for data evaluation. Electrochemically induced difference spectra were recorded and processed as previously described (*25*).

RESULTS

Effect of E272 Mutations on QCR Stability and Function. The E272D and E272Q substitutions were introduced into the *S. cerevisiae* cytochrome *b* gene by site-directed mutagenesis and biolistic bombardment. The characteristics of mutant strains and QCR variants are listed in Table 1. Both mutations (E272D and E272Q) did not abolish respiration as shown by the mutants' ability to grow on nonfermentable carbon sources. Both mutants have the same growth yield as the wild-type strain (data not shown). However, monitoring the growth in nonfermentable media revealed that the strain carrying the E272Q mutation has severe growth defects as deduced from its increased doubling time of 9.4 h. The doubling time of the E272D strain (3.4 h) was only slightly increased compared to that of the wild-type strain (3.2 h). Sequencing of the cytochrome *b* gene from mitochondrial DNA preparations prepared at different growth phases confirmed that no reversion of the E272Q mutation occurred (data not shown).

Mitochondrial membranes of E272D and E272Q prepared from yeast cells harvested at the late exponential growth phase exhibited a decrease of ~50% in QCR content measured by redox-spectroscopic analysis of the *b* heme content. The mutations may cause increased sensitivity to proteolytic cleavage. However, SDS−PAGE and Western blot analysis of the subunits cytochrome c_1, ISP, and Qcr8p of wild-type and variant mitochondrial membranes indicated no loss of subunits or assembly defects that could account for the diminished QCR content (data not shown). E272D and E272Q could both be stably purified by the standard procedure. No loss of subunits or of activity was observed during purification as judged from SDS−PAGE and Western blot analysis, redox-spectroscopical heme quantification, and enzymatic activity assays performed at different stages of the procedure (data not shown). The cytochrome *c* reductase activity of the fully purified complexes was compared. The E272D variant exhibited a 49% lower turnover number (TN) of 26 ± 3 s^{-1} than the wild-type complex (TN of 52 ± 5 s^{-1}). At first glance, the TN of E272D does not correspond to the only slightly elevated doubling time of the mutant strain in respiratory media. However, a metabolic control analysis showed that respiration and QCR do not exclusively control the growth rate (*28*). The TN of the E272Q variant was drastically affected; with a value of 7 ± 1 s^{-1}, only 13% of wild-type TN is present, indicating that QCR became a rate-limiting step. However, the low cytochrome *c* reductase activity observed for E272Q is apparently sufficient to support respiratory growth.

Binding of Decylubiquinol. To determine the impact of the side chain substitutions on substrate binding, ubiquinol:cytochrome *c* reductase activity of the purified wild-type and variant QCRs was measured in the presence of varying concentrations of decylubiquinol (DQH). The measurements were performed with the complexes reconstituted in liposomes, as quantitative binding of lipophilic ligands is more accurately assessed in this state than in the detergent-solubilized complex. Furthermore, DQH concentrations were kept below 50 μM to avoid micelle formation of the substrate. Both variants showed decreased K_m values for DQH compared to that of the wild-type enzyme. For the latter, a K_m value of 6.3 μM was determined, whereas E272Q and E272D exhibited K_m values of 3.2 and 0.9 μM, respectively. It should be noted that the parameter K_m is very complex in QCR as the catalytic turnover is a combined mechanism of quinol oxidation at center P and quinone reduction at center N. In addition, the rate constant for ubiquinol oxidation contributes to the K_m. Thus, the latter cannot be interpreted as a dissociation constant or as a direct measure of the affinity for the substrate. However, the observed changes clearly indicate that the binding and the utilization of the substrate ubiquinol at center P are affected by the E272 mutations.

Binding of Center P Inhibitors. For further analysis of alterations in the center P substrate binding pocket, the efficacy of the two distal-niche inhibitors stigmatellin and HDBT and of the proximal-niche inhibitor myxothiazol was analyzed by monitoring the influence of increasing inhibitor concentration on cytochrome *c* reductase activity of wild-type and variant QCRs. The assay was carried out with the enzymes reconstituted in liposomes to ensure accurate measurements.

In the crystal structure of yeast QCR with bound stigmatellin, E272 acts as direct ligand of the inhibitor via its carboxylate group [Figure 1b (*1*)]. Aspartate or glutamine substitution results in resistance to stigmatellin which is evident from the undisturbed cytochrome *c* reductase activity of the variants E272D and E272Q with increasing concentrations of the inhibitor (Figure 2a). Even addition of a 2×10^3-fold stoichiometric excess of the inhibitor showed no effect on the two variants (not shown), whereas addition of a stoichiometric amount of stigmatellin to the wild-type enzyme inhibited the activity by >90%. The observed resistance of the two E272 variants clearly reflects the importance of this residue for the binding of stigmatellin.

HDBT binding induces a different conformation of the E272 side chain. In the crystal structure of wild-type yeast QCR with bound heptyl-HDBT (HHDBT), the backbone nitrogen atom of E272 coordinates HHDBT via a water molecule and the glutamate side chain is rotated out of the pocket [Figure 1b (*9*)]. HDBT inhibits QCR turnover without a marked effect of the aliphatic side chain length (*29*). In this study, tridecyl-HDBT (THDBT) was used. The substitutions at position 272 did not confer resistance to THDBT as can be deduced from an increasing level of inhibition of QCR activity upon addition of increasing concentrations of the inhibitor (Figure 2b). Determination of the relative inhibitor titer [$I_{50}^r = IC_{50}$(variant)/IC_{50}(wild type)] even suggests that both variants are slightly more sensitive to THDBT as indicated by an I_{50}^r value of <1 (Table 1). This result strongly

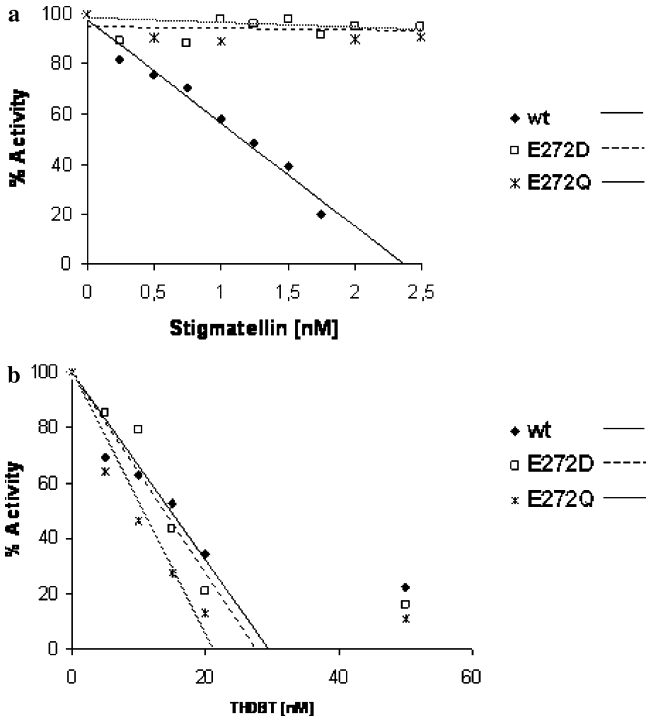

FIGURE 2: Relative inhibition of wild-type (wt) and variant QCR by (a) stigmatellin and (b) THDBT. Ubiquinol:cytochrome *c* reductase activities of wild-type and variant QCRs reconstituted in liposomes were measured in the presence of increasing concentrations of inhibitor (10 nM QCR). The activities without inhibitors were used as 100%: 52, 7, and 25 s^{-1} for the wild type, E272Q, and E272D, respectively. For each inhibitor concentration, an average of five assays was used, and standard deviations are in the range of 5−11%.

suggests that the mutations at position 272 did not drastically alter the distal niche of the center P binding pocket.

When the proximal-niche inhibitor myxothiazol was used to probe, the activity of the variant enzymes decreased upon addition of the inhibitor in the same manner as in the wild-type enzyme (data not shown). In the crystal structure of bovine QCR with myxothiazol bound to center P, the backbone amide of E271 (yeast 272) forms a hydrogen bond with the amide oxygen atom of the inhibitor (*11*). The sensitivity of the E272 variants to myxothiazol documents that the mutation did not markedly alter the proximal niche.

In QCR structures with bound stigmatellin, HDBT, or myxothiazol, the side chain of E272 is found in different orientations (*1*, *9*, *11*). The substitutions apparently also did not affect the flexibility of the side chain as both THDBT and myxothiazol bind to the variant QCRs.

Redox Potentiometry. Potentiometric redox titrations were carried out to evaluate possible effects of the side chain substitutions on the redox potentials of the heme groups. The midpoint potentials of the *b* hemes were well separated, and no major changes were observed. The E_m of heme b_L was found to be −47 mV for the wild type and −42 and −48 mV for the E272Q and E272D variants, respectively. Shifts from the heme b_H wild-type potential at 53 mV did not exceed 20 mV. Therefore, the decreased QCR turnover number in both E272 variants cannot be attributed to a modification of the *b* heme properties. As expected, the midpoint potentials of the c_1 hemes were not affected (data not shown).

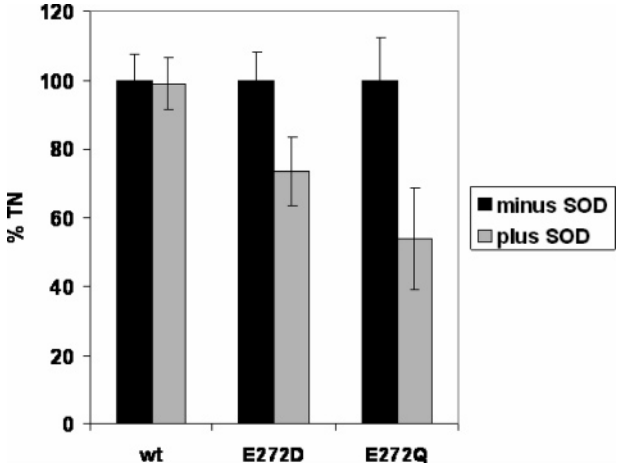

FIGURE 3: Superoxide production in the wild type (wt) and E272 variants. The rate in the absence of SOD (black bars) is the 100% value. The decreased rate with SOD included in the assay is depicted with gray bars. The assay was carried out according to the standard protocol with 10 nM QCR, 50 μM cytochrome *c*, and 40 μM decylubiquinol supplemented with 50 units/mL catalase and 50 units/mL CuZnSOD. The values are the average of five measurements. The rates in the absence of SOD for the wild type, E272Q, and E272D are 52, 7, and 25 s^{-1}, respectively.

Superoxide Production. The electron bifurcation upon ubiquinol oxidation at center P needs to be strictly controlled to prevent electron short-circuit reactions that result in superoxide formation (*5*, *6*, *13*, *30*−*32*). To analyze the influence of E272 substitutions on this process, superoxide formation of QCR was assayed as the superoxide dismutase (SOD)-sensitive rate of the cytochrome *c* reductase activity of the enzyme (*33*). The difference between the reaction rate in the absence and presence of SOD yields the contribution of the cytochrome *c* reduction by superoxide to the overall observed cytochrome *c* reductase activity. In the wild-type enzyme, virtually no superoxide formation was detected. Apparently ∼30 and ∼50% of the cytochrome *c* reduction in E272D and E272Q, respectively, can be attributed to superoxide (Figure 3). The highly enhanced generation of superoxide in the E272 variants suggests that this residue has an impact on accurate electron bifurcation.

H^+/e^- Stoichiometry. Four protons are released at center P upon oxidation of one ubiquinol according to the net balance of the Q-cycle (*5*). Uncoupling of the Q-cycle is characterized by a lowered H^+/e^- stoichiometry. The latter was determined for reconstituted wild-type and variant QCR by oxidant-pulse experiments, in which the proton release at the side of center P is monitored (Table 1). A H^+/e^- ratio of 2.01 was measured for the wild-type enzyme. E272Q and E272D have ratios of 1.97 and 1.98, respectively, i.e., within the deviation of the wild-type ratio and the experimental error. The replacement of E272 with glutamine and aspartate did not alter the ratio coinciding with the consideration that superoxide anion formation at center P is unlikely to affect proton release upon ubiquinol oxidation. However, this type of bypass reactions should lower the level of proton uptake at center N and thus the pump efficiency. In agreement, lower respiratory control rates of 3.3−3.9 were determined for E272D and E272Q compared to a rate of 4.2−4.5 for wild-type QCR.

pH Dependence of the Turnover. Three protonatable groups are rate-limiting for catalysis in bovine heart QCR (*23*). Among those, the pK_a of ∼5.7 was assigned to E272. To challenge this assumption, turnover of wild-type, E272D, E272Q QCR was monitored at different pH values and varying concentrations of DQH. A typical profile of the pH-dependent turnover of the wild type and the two variants is shown in Figure 4. Nearly no cytochrome *c* reduction for E272D and E272Q at pH <6 could be detected. The wild-type enzyme showed in the same pH range already ∼30% of the maximum turnover observed at pH 7.5. The same differences between the wild type and E272D and E272Q variants in the pH-dependent turnover profiles at pH <6 were observed for four additional DQH concentrations (4, 8, 24, and 32 μM, data not shown). At pH >6, the turnover number of E272D and E272Q increased and reached its maximum at pH ∼7.5 and decreased again for higher pH values, as did the wild-type activity. In the pH range of 6−9.5, the variants E272D and E272Q exhibit a pH profile similar to that of the wild-type enzyme for all DQH concentrations (data not shown).

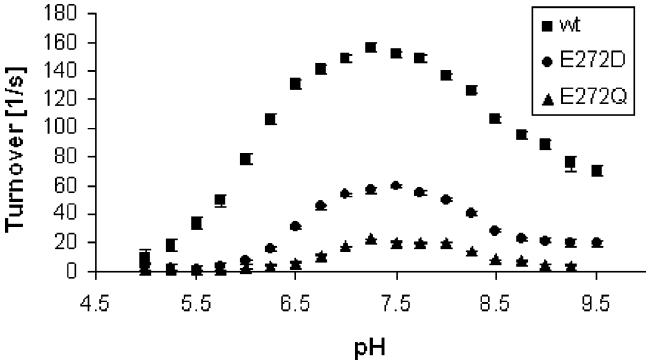

FIGURE 4: pH dependence of the turnover rate of cytochrome *c* reduction at 16 μM DQH. The averages of four to six separate experiments with two different enzyme preparations with their corresponding standard error are shown.

Differences between the wild-type and variant QCRs can be specified by determining the apparent pK_a values from the pH profiles. The apparent catalytic constant of the reaction ($k_{cat,obs}$) was determined for each pH value that was monitored. The values for $k_{cat,obs}$ were calculated by fitting the data obtained for the different DQH concentrations for each pH value to the Michaelis−Menten equation. The plot of log $k_{cat,obs}$ versus H^+ concentration for the wild-type enzyme, E272D, and E272Q was fitted with the following two equations according to the method of Covian and Moreno-Sanchez (Figure 5a−c).

$$\log k_{cat,obs} = \log\left[\Delta k_{cat}\left(1+\frac{[H^+]}{\alpha K_{a1}}\right)+k_{cat}\left(\frac{\beta[H^+]^2}{\alpha K_{a1}K_{a2}}\right)\right] - \log\left(1+\frac{[H^+]}{\alpha K_{a1}}+\frac{[H^+]^2}{\alpha K_{a1}K_{a2}}+\frac{[H^+]^3}{\alpha\gamma K_{a1}K_{a2}K_{a3}}\right) \quad (1)$$

$$\log k_{cat,obs} = \log\left[\Delta k_{cat}\left(1+\frac{[H^+]}{\alpha K_{a1}}\right)\right] - \log\left(1+\frac{[H^+]}{\alpha K_{a1}}+\frac{[H^+]^2}{\alpha\gamma K_{a1}K_{a2}}\right) \quad (2)$$

Equation 1 describes the dependence of $k_{cat,obs}$ of three pK_a values. Equation 2 represents a two-pK_a model. The data for the wild-type enzyme showed the best fit for eq 1 (Figure

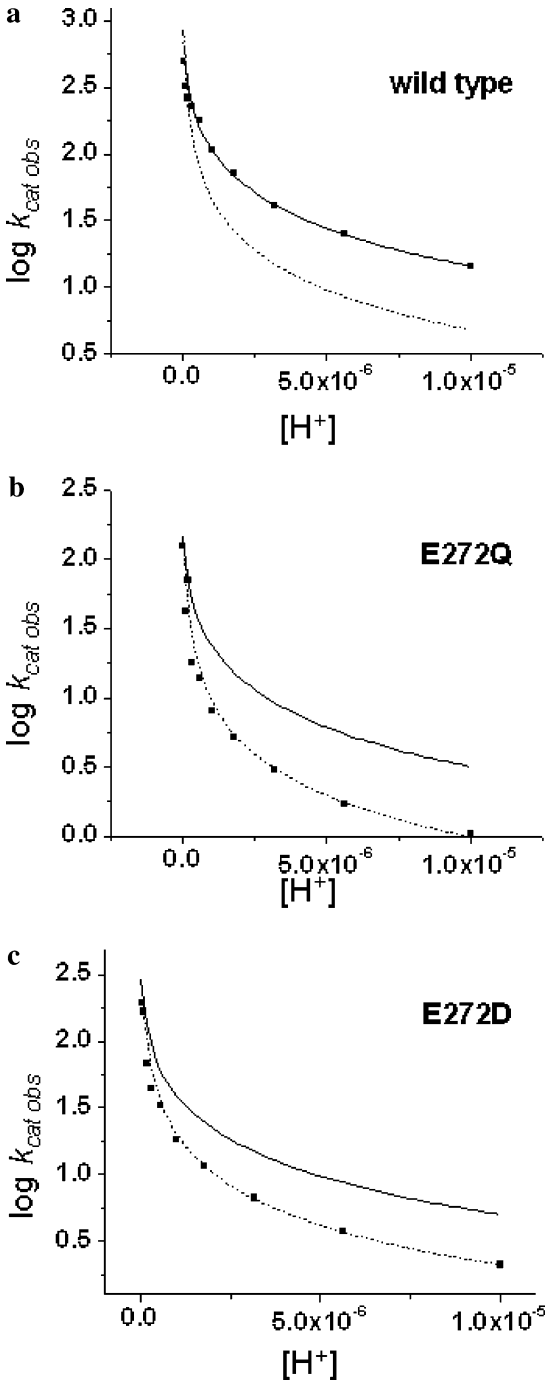

FIGURE 5: Plots of log $k_{cat,obs}$ vs proton concentration for the wild type (a), E272Q (b), and E272D (c). The log $k_{cat,obs}$ plot was fitted to eq 1 with three (—) and to eq 2 with two (···) pK_a values. See Table 2 for the values. $k_{cat,obs}$ was calculated by fitting the turnover number at 4, 8, 16, 24, and 32 μM DQH for each pH to the Michaelis−Menten equation.

5a). The obtained pK_a values for the wild-type enzyme (pK_{a1} = 9.5, pK_{a2} = 7.5, and pK_{a3} = 6.2) are in good agreement with the previously reported values for bovine QCR (pK_{a1} = 9.2, pK_{a2} = 7.5, and pK_{a3} = 5.7) (*23*). Fitting of the E272D and E272Q data to eq 1 (three pK_a values) was possible only if large deviations were tolerated (see panels b and c of Figure 5). The latter included large standard deviations for all variants (up to 100 times the estimated value) and negative values for one or more variants. In addition, only the chosen fitting yielded respective $k_{cat,obs}$ ratios of variants to wild type comparable to the steady-state measurements. In contrast,

Table 2: Values Derived from Fitting Data in Figure 5

	k_{cat} (s^{-1})	β	pK_{a1}[a]	pK_{a2}[b]	pK_{a3}[c]
wild type	1480 ± 132	0.17 ± 0.03	9.5 ± 0.2	7.5 ± 0.1	6.2 ± 0.3
E272Q	307 ± 68	-	9.3 ± 0.3	7.3 ± 0.3	-
E272D	621 ± 97	-	9.2 ± 0.3	7.4 ± 0.1	-

[a] Corresponds to $p\alpha K_{a1}$. [b] Corresponds to $p\gamma K_{a2}$. [c] Corresponds to $p\gamma K_{a3}$.

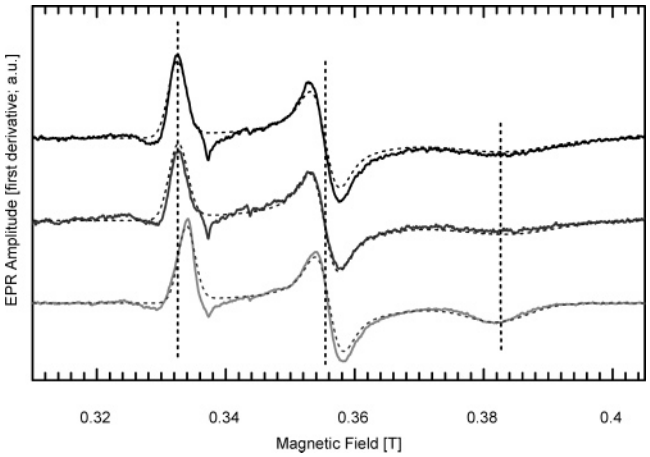

FIGURE 6: Center P probed by electron paramagnetic resonance (EPR) spectra of the ISP [2Fe-2S] cluster. EPR spectra of a 20 μM protein solution reduced with a 1000-fold excess of pyrophosphate-buffered dithionite were recorded. Spectra of purified wild-type (top), E272Q (middle), and E272D (bottom) QCR are shown. Values for g_{xx}, g_{yy}, and g_{zz} are listed in Table 3.

Table 3: Values for the **g** Tensor of the Dithionite-Reduced ISP in Wild-Type and Variant QCR[a]

	wild type	E272Q	E272D
g_{zz}	2.025	2.024	2.017
g_{yy}	1.894	1.895	1.891
g_{xx}	1.753	1.749	1.761

[a] The error is ±0.003 for all g values.

the two-pK_a curve yielded the best fit for both variants. The obtained pK_a values for E272D (pK_{a1} = 9.2 and pK_{a2} = 7.4) and E272Q (pK_{a1} = 9.3 and pK_{a2} = 7.3) are close to the obtained pK_{a1} and pK_{a2} values determined for the wild-type enzyme (see Table 2). Apparently, the catalysis of the E272 variants shows a pH profile different from that of the wild-type enzyme. The alteration is most pronounced below pH 6.5, and the pH dependence of $k_{cat,obs}$ could be best described by two pK_a values. Compared to that of the wild-type enzyme, the third apparent pK_{a3} of 6.2 is redundant in E272D and E272Q.

Center P Occupancy Monitored by EPR Analysis. The EPR signal of the reduced ISP varies with the redox state of the quinone pool and with the inhibitor occupancy of center P (*34*). The g_{xx} signal of the reduced ISP is attributed to interaction between ISP and the quinol binding pocket (*35*). Changes in the shape and position of the signals can be interpreted as alterations of the interaction of ISP with center P.

Continuous-wave EPR spectra of detergent-solubilized purified QCR were recorded. Both variants share similar features with the wild-type enzyme with regard to the position and shape of the signals in the spectra of the dithionite-reduced probes (Figure 6 and Table 3). The spectra for E272Q and wild-type QCR are nearly identical, while

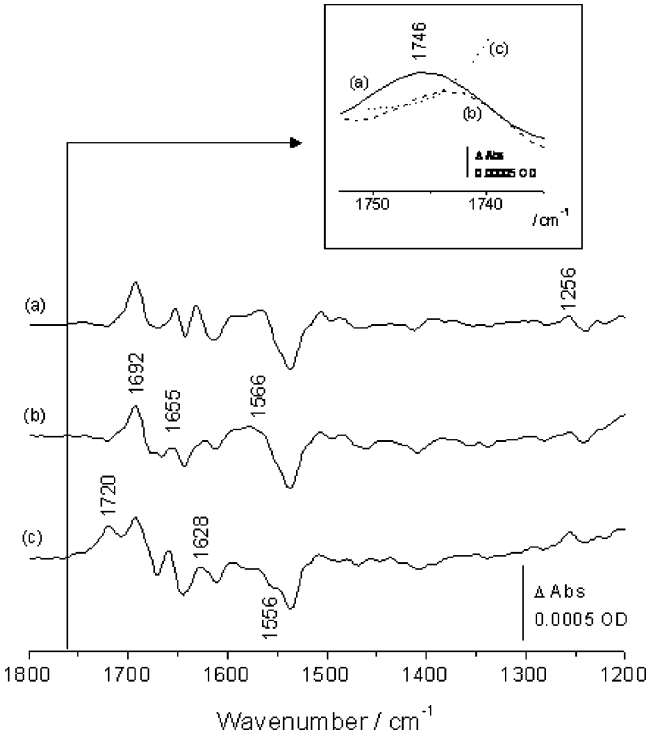

FIGURE 7: Oxidized-minus-reduced FTIR difference spectra of wild-type (a), E272Q (b), and E272D (c) QCR. The inset shows the enlarged view of the spectral range from 1750 to 1735 cm^{-1}.

the g_{xx} signal in E272D marked by a vertical line in Figure 6 differs both in line shape and position from those of the wild type and E272Q. For the latter two, the signal is slightly broader and found at a higher field, whereas the peak for E272D is narrower and shifted to a lower magnetic field. Moreover, the g_{zz} signal of E272D is also markedly shifted to a higher magnetic field compared to those of the wild-type and E272Q enzymes. This shift may indicate a structural change within the center P binding pocket in the environment of the ISP.

To monitor the influence of ubiquinol saturation on the g_{xx} band, antimycin-inhibited samples with a 100-fold excess of ubiquinol were measured. The inhibitor antimycin binds specifically and with high affinity to center N and thus prevents quinol−quinone exchange with center P. Upon addition of antimycin and quinol, no major changes in the wild type or E272Q variant were observed. The above-described g_{zz} shift for E272D is partially reversed, while the differences in g_{xx} remain (data not shown).

For none of the complexes was a major difference between ascorbate- and dithionite-reduced samples noted (data not shown).

Redox-Induced FTIR Spectroscopy. For further characterization, redox-induced FTIR difference spectroscopic studies were performed with detergent-solubilized purified QCR (Figure 7). Intensity changes in the amide I region at 1652 and 1632 cm^{-1} as well as in the amide II region at 1550−1450 cm^{-1} are observed in a comparison of the spectra of wild-type and variant QCR. These changes include signals from the polypeptide backbone and may thus reflect structural changes induced by the mutations that are addressed by the redox reaction. In addition, perturbations of individual amino acids are likely. At 1746 cm^{-1}, a clear peak is observed in the wild-type spectra (*36*), together with a small negative signal at 1727 cm^{-1}. The spectral region above 1710 cm^{-1} is characteristic for the ν(C═O) vibration of protonated aspartic and glutamic acids (*37*). The signals observed here for wild-type QCR reflect the contribution of at least one aspartic or glutamic acid protonated in the oxidized form (1746 cm^{-1}) and one residue protonated in the reduced form (1727 cm^{-1}). Deprotonation of the acid can be observed at 1566 and 1439 cm^{-1} for the $\nu(COO^-)^{as,s}$ vibrational modes. A clear assignment of the peak at 1746 cm^{-1} was not possible previously, and the contribution of other residues in the binding pocket, e.g., E66, was discussed (*36*).

In the FTIR difference spectra of E272Q (Figure 7b and Figure 7 inset), a clear loss of intensity at 1746 cm^{-1} is seen. This indicates that the contribution of a protonated aspartic or glutamic acid is lost. Comparison with the wild-type spectra suggests that the peak at this position in the wild-type spectra is caused by protonated E272. In the spectra of E272D (Figure 7c), the intensity at 1746 cm^{-1} was lost and a new peak for a carbonyl vibration at higher wavenumbers was observed. This new signal could include the contribution of the introduced aspartate upshifted due to a weaker hydrogen bonding or of a different acidic residue from the binding pocket, protonated as a result of structural changes in the variant.

Further differences relevant for protonation reactions are reflected in deviations of absorption in the regions for the $(COO^-)^{as}$ mode at 1566 cm^{-1} and the $(COO^-)^{s}$ mode at 1439 cm^{-1}. In both positions, intensity is lost in the E272Q variant. In the E272D variant, strong variations around 1720 and 1550 cm^{-1} as well as in the amide I region can be seen, indicating structural changes in the mutant enzyme.

DISCUSSION

E272 of the conserved cytochrome *b* PEWY motif has been suggested as a ubiquinol ligand and proton acceptor for the yet unknown enzyme−substrate complex at center P of QCR. We introduced the two replacement mutations, E272D and E272Q, into the mitochondrially encoded cytochrome *b* gene by biolistic transformation to study the effects on substrate binding and catalysis.

The resulting variants were able to grow on nonfermentable carbon sources, but E272Q had a slower growth rate. This effect coincides with a lowered QCR turnover number, which is reduced by half for the E272D variant and in a more pronounced manner (by 87%) for E272Q. A similar effect was seen in bacterial QCR. The equivalent variants in *Rhodobacter sphaeroides* (E295D and E295Q) yielded only 11% of the wild-type quinol oxidation rate for the aspartate and <4% for the glutamine substitution when the rates were measured in membranes (*13*). Clearly, aspartate and glutamine substitutions of E272 disturb QCR activity, and the effect is more pronounced for the latter, indicating that the charge at this position is important for catalysis. What is the molecular basis of this effect: is it a direct interference with quinol oxidation? Indirect effects due to perturbations of the heme environment can be excluded, as the mutations caused no major changes in the midpoint potentials of the two *b* hemes. In the *Rh. sphaeroides* E295Q variant, the potential of heme b_L was lowered by 30 mV (*38*).

Structural alterations in the quinol binding pocket were probed with center P-specific inhibitors. Resistance against

stigmatellin was observed in reconstituted E272D and E272Q variants, but sensitivity toward the proximal inhibitor myxothiazol was retained. Stigmatellin resistance was also reported for the bacterial equivalents (*13*, *39*). Clearly, the E272 carboxylate group and its exact position are important for binding of stigmatellin. Both variants exhibited high, even slightly increased, sensitivity to the distal center P inhibitor THDBT. In the X-ray structure of yeast QCR, HHDBT is coordinated by the NH backbone of E272. The inhibitor binds in its ionized form, and the glutamate side chain is rotated outward (*9*). Therefore, HDBT binding is independent of the side chain at position 272 and requires conformational freedom only so that the observed coordination pattern of the wild-type enzyme can be maintained. The retained sensitivity to the distal center P inhibitor THDBT indicates that the mutations do not evoke large structural rearrangements. More importantly, the substitution did not affect the flexibility of the side chain, as can be deduced from the binding of both THDBT and myxothiazol, which require different orientations of the side chain. The flexibility at this position is thought to be important for ubiquinol oxidation. Existing models for the quinol oxidation rely on a reorientation of E272 (*5*, *9*, *13*, *16*). In both variants, this flexibility is apparently retained, which allows us to focus on the influence of shortening the side chain and of substituting carboxylate with amide on the mechanism of the enzyme.

On the basis of the coinciding binding sites of stigmatellin and quinone in the bacterial reaction center (*40*), the stigmatellin-bound QCR has been proposed to mimic the enzyme−substrate complex with ubiquinol or a reaction intermediate at center P (*1*, *5*, *9*, *13*). The observed inhibitor resistance for E272Q and E272D may therefore mirror a perturbed binding of the substrate ubiquinol resulting in the lowered QCR activity. In agreement with this consideration, the enhanced superoxide production in the two E272 variants indicates a disturbed quinol enzyme−substrate complex. Improper binding of both ubiquinol and ISP to the binding pocket is thought to allow electron short-circuit reactions resulting in superoxide formation (*30*, *31*, *33*). Though the data clearly indicate a disturbed enzyme−substrate complex, one has to question whether it is a direct effect of E272 or whether structural perturbations occur in the quinol binding pocket.

If the glutamate side chain is the direct ligand of ubiquinol, shortening the side chain by aspartate substitution as well as neutralization to glutamine will destabilize the substrate and alter its position in the binding pocket. This will consequently disturb the enzyme−substrate complex that is formed by the cytochrome *b* portion of the binding pocket, ubiquinol, and ISP docked in the *b* position. This view is supported by the EPR analysis of the reduced ISP. In the purified enzyme, E272D has signals different from those of the wild-type enzyme indicating changes in the environment of the reduced ISP. These changes may be caused by structural perturbations at center P and/or by a disturbed binding mode of ubiquinol. Both phenomena could influence the electronic environment of the ISP, thus leading to shifts in the EPR signals. Interestingly, the EPR spectra of the reduced ISP in the E272Q variant coincide with the signals of the wild-type enzyme, indicating that the electronic environment in this variant remains unperturbed.

Different effects of the aspartate and glutamate substitution can be observed not only in the EPR spectra of the reduced ISP but also in the pre-steady-state heme reduction kinetics. Here, the reduction yield of the high- and low-potential chain in the E272Q variant is unchanged compared to that of the wild-type enzyme, but electron transfer in this variant occurs at a slower rate. In contrast, E272D shows a decreased rate and a reduced yield for both chains (unpublished results).

The pH profile of E272D and E272Q clearly differs from that of the wild-type enzyme. At pH <6, catalysis in the two variants is nearly abolished in contrast to that in wild-type QCR. In the pH range from 6 to 9.5, the profile of the variants is similar to that of the wild-type enzyme. Apparently, a proton exchange step becomes rate-limiting in E272D and E272Q at pH <6 in contrast to that of the wild-type enzyme, whereas no differences in rate limitation occur at pH >6. This difference in the pH profile is presumably caused by the loss of a protonatable group. In yeast wild-type QCR (this study) and in bovine QCR (*23*), three protonatable groups affect catalysis. The determined pK_a values are in good agreement, and the assignment of the lowest pK_a to E272 was suggested for the bovine system. This pK_a is lost in both E272 variants, as the pH dependence of $k_{cat,obs}$ can be fully described by the two other pK_a values, which are not affected by the substitutions. This supports the pK_a assignment and clearly points to an important role of E272 in proton exchange. One has to note that E272D exhibits a pH profile similar to that of E272Q, although the aspartate side chain is in principle protonatable in contrast to the latter. One may speculate that the shorter side chain in E272D perturbs proton exchange and thereby affects the rate of catalysis in a manner similar to that of E272Q.

The consequences of the two substitutions clearly mark E272 as an important residue for center P catalysis, and the following interpretation appears plausible. In E272D, the shorter side chain apparently affects the ubiquinol binding position and thereby the interaction with ISP, as verified by alteration of the **g** tensors observed by EPR. This coincides with an altered K_m for decylubiquinol, a lowered QCR activity, and enhanced superoxide formation. In contrast, the EPR spectra indicate that in E272Q the ISP binding appears to be undisturbed and the reduction of the high-potential chain is largely unchanged. However, the markedly lower QCR activity, the altered K_m for decylubiquinol, and the extent of superoxide generation, which is even higher than in E272D, indicate that the ubiquinol oxidation is disturbed. It is possible that the position of ubiquinol and, thus, the ISP environment are not affected but that the substitution perturbs electron bifurcation. The substitution does not provoke major changes in the architecture of the binding pocket and in the side chain flexibility as judged by inhibitor titrations, nor does it alter the *b* heme potentials. Thus, the effects arise from the substitution of glutamate with glutamine. The suggested role for E272 is to accept the proton released upon ubiquinol oxidation and to deliver it in the direction of heme b_L parallel to the electron in a proton-coupled electron transfer (*1*, *9*, *13*, *14*). We suggest that substitution of the carboxylate with an amide abolishes this proton transfer in the E272Q variant and may thereby disturb electron transfer. The low-potential chain part of ubiquinol oxidation is thus likely the source of the electron short-circuit reaction as detected by superoxide production in the E272Q

variant. However, the E272Q substitution is not lethal; residual QCR activity is retained, and the H^+/e^- ratio remains unchanged (Table 1), indicating that other protonatable residues in the vicinity such as H253 (*9*) provide an alternative route for proton exit. This alternative is not sufficient for pH values lower than 6.5, at which hardly any QCR activities could be detected for E272D and E272Q. Glutamate at position 272 is fully conserved in mitochondrial cytochrome *b* (*41*), and replacements in the conserved PEWY loop do not occur randomly but are linked to a few phylogenetic clades (*42*). It has been proposed that in all organisms with a valine or a proline as an equivalent to E272, there is a glutamate in various positions of the *ef* loop, which may compensate for the exchange (*43*). On the basis of a recent comprehensive phylogenetic study of "Rieske/cytochrome *b*" complexes (*44*), we suggest that in β- and γ-proteobacteria, in which the PEWY glutamate is substituted with valine or proline, a glutamate equivalent to yeast H253 is conserved (e.g., E288 in *Vibrio cholerae*), which could take over the proton transfer function. Interestingly, rotational displacement of Glu272 in the X-ray structure of the yeast cytochrome bc_1 complex with the hydroxyl quinone inhibitor HDBT is accompanied by reorientation of His253 (*9*). This brings the two neighboring side chains within 3 Å of each other. Thus, the conserved glutamate equivalent to H253 appears to be well suited to relay protons in the same manner as E272, supporting the notion of a parallel electron−proton transfer toward heme b_L. Species dependence could explain the different extent of the effects of aspartate, glutamine, and glycine substitutions of E295 (equivalent to yeast E272) in the photosynthetic purple bacterium *Rh. sphaeroides* (*13*, *38*, *39*). In cytochrome *b* of *Rh. sphaeroides*, an insertion of 18 residues, including two aspartate residues, is located 13 positions C-terminal of the PEWY loop. On the basis of the comparison with the structure of the yeast complex, one can speculate that the insertion could bring protonatable residues close to the PEWY loop and thus may partially compensate for the loss of the carboxylate function at position 295.

Clearly, the aspartate and glutamate substitutions have an effect on redox-dependent protonation changes of QCR as analyzed by redox-induced FTIR difference spectra. The indicated subtle structural changes are in line with the plasticity of center P, which was demonstrated with the comparison of the structures of stigmatellin- and HHDBT-inhibited yeast QCR (*9*). Besides the reorientation of the E272 and H253 side chains, the main differences are confined to a local Cα trace displacement (<2 Å) accompanied by an altered side chain orientation in a part (A267−V270) of the *ef* loop (Figure 1b). The side chain substitutions may have an effect at a similar level. The weakening of the signal at 1746 cm^{-1} characteristic of protonated acidic residues in E272Q and its frequency upshift for E272D point to a direct involvement of this residue. Since alterations are present in the area for deprotonated signals as well as for structural changes, an indirect effect of the substitutions with respect to the 1746 cm^{-1} signal cannot be excluded. It should be noted that the QCR preparations have a low quinone content. Thus, the side chain can be rotated into the binding pocket of center P, as seen in the QCR crystal structure of QCR with nonoccupied center P (*15*). Studies with bound HDBT aimed at further investigating this signal in wild-type and variant QCRs are in progress.

In conclusion, aspartate and glutamate substitutions of E272 do affect binding and oxidation of ubiquinol, promote electron short-circuit reactions, and alter the pH dependence of ubiquinol oxidation. The residue appears to be important for the accurate molecular construction of the enzyme−substrate complex and for prevention of electron short-circuit reactions, which would limit the efficiency of the enzyme and would produce deleterious reactive oxygen species. The carboxylate position may steer the binding position of the ubiquinol and thereby the proper docking of the ISP to center P. The altered pH profile in both E272D and E272Q, which can be explained by the loss of a protonatable group with a pK_a of ∼6, supports the suggested role of E272 in proton exchange. Further studies are required to exclude possible indirect effects and to challenge the role of E272 as a direct ligand of ubiquinol.

ACKNOWLEDGMENT

We thank Prof. B. L. Trumpower for the gift of HDBT and THDBT, Dr. Raul Covian for the help with the pK_a determination, and W. Nitschke for providing and discussing the Rieske/cytochrome *b* complex study prior to publication.

REFERENCES

1. Hunte, C., Koepke, J., Lange, C., Rossmanith, T., and Michel, H. (2000) Structure at 2.3 Å resolution of the cytochrome bc_1 complex from the yeast *Saccharomyces cerevisiae* co-crystallized with an antibody Fv fragment, *Structure 8*, 669−684.
2. Hunte, C., Palsdottir, H., and Trumpower, B. L. (2003) Protonmotive pathways and mechanisms in the cytochrome bc_1 complex, *FEBS Lett. 545*, 39−46.
3. Mitchell, P. (1976) Possible molecular mechanisms of the protonmotive function of cytochrome systems, *J. Theor. Biol. 62*, 327−367.
4. Zhang, Z., Huang, L., Shulmeister, V. M., Chi, Y. I., Kim, K. K., Hung, L. W., Crofts, A. R., Berry, E. A., and Kim, S. H. (1998) Electron transfer by domain movement in cytochrome bc_1, *Nature 392*, 677−684.
5. Crofts, A. R. (2004) The cytochrome bc1 complex: Function in the context of structure, *Annu. Rev. Physiol. 66*, 689−733.
6. Ocyczka, A., Moser, C. C., Daldal, F., and Dutton, P. L. (2004) Reversible redox energy coupling in electron-transfer chains, *Nature 427*, 607−612.
7. Rich, P. R. (2004) The quinone chemistry of bc complexes, *Biochim. Biophys. Acta 1658*, 165−171.
8. von Jagow, G., and Link, T. A. (1986) Use of specific inhibitors on the mitochondrial bc_1 complex, *Methods Enzymol. 126*, 253−271.
9. Palsdottir, H., Lojero, C. G., Trumpower, B. L., and Hunte, C. (2003) Structure of the yeast cytochrome bc_1 complex with a hydroxyquinone anion Q_o site inhibitor bound, *J. Biol. Chem. 278*, 31303−31311.
10. Kim, H., Xia, D., Yu, C. A., Xia, J. Z., Kachurin, A. M., Zhang, L., Yu, L., and Deisenhofer, J. (1998) Inhibitor binding changes domain mobility in the iron−sulfur protein of the mitochondrial bc1 complex from bovine heart, *Proc. Natl. Acad. Sci. U.S.A. 95*, 8026−8033.
11. Esser, L., Quinn, B., Li, Y.-F., Zhang, M., Elberry, M., Yu, L., Yu, C.-A., and Xia, D. (2004) Crystallographic studies of quinol oxidation site inhibitors: A modified classification of inhibitors for the cytochrome bc_1 complex, *J. Mol. Biol. 341*, 281−302.
12. Hauska, G., Nitschke, W., and Hermann, R. G. (1988) Amino acid identities in the three redox center-carrying polypeptides of cytochrome bc_1/b_6f complexes, *J. Bioenerg. Biomembr. 20*, 211−228.
13. Crofts, A. R., Hong, S., Ugulava, N., Barquera, B., Gennis, R., Guerova-Kuras, M., and Berry, E. (1999) Pathways for proton release during ubihydroquinone oxidation by the bc_1 complex, *Proc. Natl. Acad. Sci. U.S.A. 96*, 10021−10026.
14. Crofts, A. R., Barquera, B., Gennis, R. B., Kuras, R., Guergova, K., and Berry, E. A. (1999) Mechanism of ubiquinol oxidation

by the bc_1 complex: Different domains of the quinol binding pocket and their role in the mechanism and binding of inhibitors, *Biochemistry 38*, 15807−15826.
15. Iwata, S., Lee, J. W., Okada, K., Lee, J. K., Iwata, M., Rasmussen, B., Link, T. A., Ramaswamy, S., and Jap, B. K. (1998) Complete structure of the 11-subunit bovine mitochondrial cytochrome bc_1 complex, *Science 281*, 64−71.
16. Mulkidjanian, A. Y. (2005) Ubiquinol oxidation in the cytochrome bc_1 complex: Reaction mechanism and prevention of short-circuiting, *Biochim. Biophys. Acta 1709*, 5−34.
17. Bonnefoy, N., and Fox, T. D. (2001) Genetic transformation of *Saccharomyces cerevisiae* mitochondria, *Methods Cell Biol. 65*, 381−396.
18. Meunier, B. (2001) Site-directed mutations in the mitochondrially encoded subunits I and III of yeast cytochrome oxidase, *Biochem. J. 354*, 407−412.
19. Hill, P., Kessl, J., Fisher, N., Meshnick, S., Trumpower, B. L., and Meunier, B. (2003) Recapitulation in *Saccharomyces cerevisiae* of cytochrome *b* mutations conferring resistance to atovaquone in *Pneumocystis jirovec*i, *Antimicrob. Agents Chemother. 47*, 2725−2731.
20. Palsdottir, H., and Hunte, C. (2003) Purification of the cytochrome bc_1 complex from yeast, in *Membrane protein purification and crystallization* (Hunte, C., von Jagow, G., and Schägger, H., Eds.) 2nd ed., pp 191−203, Academic Press, New York.
21. Leung, K. H., and Hinkle, P. C. (1975) Reconstitution of ion transport and respiratory control in vesicles formed from reduced coenzyme Q-cytochrome *c* reductase and phospholipids, *J. Biol. Chem. 250*, 8467−8471.
22. Cocco, T., Lorusso, M., Di Paola, M., Minuto, M., and Papa, S. (1992) Characteristics of energy-linked proton translocation in liposome reconstituted bovine cytochrome bc_1 complex, *Eur. J. Biochem. 209*, 475−481.
23. Covian, R., and Moreno-Sanchez, R. (2001) Role of protonable groups of bovine heart bc_1 complex in ubiquinol binding and oxidation, *Eur. J. Biochem. 268*, 5783−5790.
24. Moss, D., Nabedryk, E., Breton, J., and Mäntele, W. (1990) Redox-linked conformational changes in proteins detected by a combination of infrared spectroscopy and protein electrochemistry. Evaluation of the technique with cytochrome *c*, *Eur. J. Biochem. 187*, 565−572.
25. Hellwig, P., Ostermeier, C., Michel, H., Ludwig, B., and Mantele, W. (1998) Electrochemically induced FT-IR difference spectra of the two- and four-subunit cytochrome *c* oxidase from *P. denitrificans* reveal identical conformational changes upon redox transitions, *Biochim. Biophys. Acta 1409*, 107−112.
26. Coremans, J. M. C. C., Van der Zwaan, J. W., and Albrach, S. P. J. (1989) Redox behaviour of nickel in hydrogenase from *Methanobacterium thermoautotrophicum* (strain Marburg). Correlation between the nickel valence state and enzyme activity, *Biochim. Biophys. Acta 997*, 256−267.
27. Hellwig, P., Soulimane, T., Buse, G., and Mantele, W. (1999) Electrochemical, FTIR, and UV/VIS spectroscopic properties of the ba_3 oxidase from *Thermus thermophilus*, *Biochemistry 38*, 9648−9658.
28. Boumans, H., Berden, J. A., Grivell, L. A., and van Dam, K. (1998) Metabolic control analysis of the bc_1 complex of *Saccharomyces cerevisiae*: Effect on cytochrome *c* oxidase, respiration and growth rate, *Biochem. J. 331*, 863−877.
29. Bowyer, J. R., Edwards, C. A., Ohnishi, T., and Trumpower, B. L. (1982) An analogue of ubiquinone which inhibits respiration by binding to the iron−sulfur protein of the cytochrome bc_1 segment of the mitochondrial respiratory chain, *J. Biol. Chem. 257*, 8321−8330.
30. Muller, F., Crofts, A. R., and Kramer, D. M. (2002) Multiple Q-cycle bypass reactions at the Q_o site of the cytochrome bc_1 complex, *Biochemistry 41*, 7866−7874.
31. Muller, F. L., Roberts, A. G., Bowman, M. K., and Kramer, D. M. (2003) Architecture of the Q_o site of the cytochrome bc_1 complex probed by superoxide production, *Biochemistry 42*, 6493−6499.
32. Osyczka, A., Moser, C. C., and Dutton, P. L. (2005) Fixing the Q cycle, *Trends Biochem. Sci. 30*, 176−182.
33. Sun, J., and Trumpower, B. L. (2003) Superoxide anion generation by the cytochrome bc_1 complex, *Arch. Biochem. Biophys. 419*, 198−206.
34. Samoilova, R. I., Kolling, D., Uzawa, T., Iwasaki, T., Crofts, A. R., and Dikanov, S. A. (2002) The interaction of the Rieske iron−sulfur protein with occupants of the Q_o-site of the bc_1 complex, probed by electron spin−echo envelope modulation, *J. Biol. Chem. 277*, 4605−4608.
35. Ding, H., Moser, C. C., Robertson, D. E., Tokito, M. K., Daldal, F., and Dutton, P. L. (1995) Ubiquinone pair in the Q_o site central to the primary energy conversion reactions of cytochrome bc_1 complex, *Biochemistry 34*, 15979−15996.
36. Ritter, M., Palsdottir, H., Abe, M., Mäntele, W., Hunte, C., Miyoshi, H., and Hellwig, P. (2004) Direct evidence for the interaction of stigmatellin with a protonated acidic group in the bc_1 complex from *Saccharomyces cerevisiae* as monitored by FTIR difference spectroscopy and ^{13}C specific labeling, *Biochemistry 43*, 8439−8446.
37. Mäntele, W. (1993) Reaction-induced infrared difference spectroscopy for the study of protein function and reaction mechanisms, *Trends Biochem. Sci. 18*, 197−202.
38. Crofts, A. R., Barquera, B., Bechamnn, G., Guergova, M., Salcedo-Hernandez, R., Hacker, B., Hing, S., and Gennis, R. B. (1995) Structure and function in the BC1-complex of *Rhodobacter sphaeroides*, in *Photosynthesis: From Light to Biosphere* (Mathis, P., Ed) Vol. II, pp 493−500, Kluwer Academic Publishers, Dordrecht, The Netherlands.
39. Brasseur, G., Saribas, A. S., and Daldal, F. (1996) A compilation of mutations located in the cytochrome *b* subunit of the bacterial and mitochondrial bc_1 complex, *Biochim. Biophys. Acta 1275*, 61−69.
40. Lancaster, C. R., and Michel, H. (1997) The coupling of light-induced electron transfer and proton uptake as derived from crystal structures of reaction centres from *Rhodopseudomonas viridis* modified at the binding site of the secondary quinone, QB, *Structure 5*, 1339−1359.
41. Degli Eposti, M., de Vries, S., Crimi, M., Ghelli, A., Patarnello, T., and Meyer, A. (1993) Mitochondrial cytochrome *b*: Evolution and structure of the protein, *Biochim. Biophys. Acta 1143*, 243−271.
42. Schutz, M., Brugna, M., Lebrun, E., Baymann, F., Huber, R., Stetter, K. O., Hauska, G., Toci, R., Lemesle-Meunier, D., Tronm, P., Schmidt, C., and Nitschke, W. (2000) Early evolution of cytochrome bc complexes, *J. Mol. Biol. 300*, 663−675.
43. Brasseur, G., Bruscella, P., Bonnefoy, V., and Lemesle-Meunier, D. (2002) The bc_1 complex of the iron-grown acidophilic chemolithotrophic bacterium *Acidithiobacillus ferrooxidans* functions in the reverse but not in the forward direction. Is there a second bc_1 complex? *Biochim. Biophys. Acta 1555*, 37−43.
44. Nitschke, W., Lebrun, E, Santini, J., Brugna, M. E., Ducluzeau, A.-L., Ouchane, S., Schoepp-Cothenet, B., and Baymann, F. (2006) The Rieske protein: A case study on the pitfalls of multiple sequence alignments and phylogenetic reconstruction, *Mol. Biol. Evol.* (in press).
45. Lange, C., and Hunte, C. (2002) Crystal structure of the yeast cytochrome bc_1 complex with its bound substrate cytochrome *c*, *Proc. Natl. Acad. Sci. U.S.A. 99*, 2800−2805.

BI060280G